Technical Paper

ISSN 1997-1400 Int. J. Pavement Res. Technol. 2(4):137-147

Factors Affecting Cracking of Notched Asphalt Concrete

R. A. Tarefder[1+], E. M Kias[2], and T. Ng[3]

Abstract: This study described the testing and analysis of cracking in asphalt concrete samples in the laboratory. Semi-circular notched specimens were prepared using a Superpave Gyratory Compactor and a water-cooled masonry saw. Samples were prepared with varying material properties including air void content, mix type, and moisture condition. The specimens were tested in three-point bending and a crack was initiated at the notch tip located in the center of the flat edge of the specimen. Load and horizontal displacement data were collected in real time at different locations. The resulting load versus displacement curves for each specimen yielded parameters that were used to determine which mix type is least susceptible to crack initiation and propagation. Three different Superpave mixes with a wider range of air voids were tested under wet and dry conditions. Air voids have little effect on crack initiation and ultimate strength of a specimen, but cracks propagated faster in specimens with higher air voids. Wet samples were shown to resist failure due to cracking by exhibiting increased ductility, yet the slope of the crack propagation curve revealed that damage due to crack propagation is more extensive in wet samples. Cracking caused more damage in coarser mixes due to increased interface cracking.

Key words: *Asphalt mix; Cracking; Moisture; Notch; Semicircular.*

Introduction

Hot Mix Asphalt (HMA) pavement constitutes a sizeable portion of the United States Department of Transportation's annual expenditure on construction and rehabilitation of the country's pavement infrastructure. Cracking is one of the major distresses of HMA pavements. Cracks in HMA provide a pathway for water, which can lead to damage in the form of asphalt stripping from the aggregate surface and softening of the mastic. Cracking contributes to a decrease in HMA pavement's serviceability, which in turn increases pavement maintenance and reconstruction costs. This study focuses on laboratory characterization of cracking in asphalt concrete.

In the last decade, permanent deformation has been controlled using Performance Grade (PG) binders and Superpave's large aggregates. However, cracking has become the inseparable biggest problem of asphalt pavements with HMA mixes designed by the Superpave method. While cracking and rutting issues should be addressed largely by pavement design consideration, they may be affected by mix design, properties, and wet/dry conditions. Properties of HMA concrete such as aggregate gradation, air voids or density, or moisture condition may affect crack initiation and crack propagation of Superpave mixes or pavements. Current standards for the approval of an asphalt concrete mix design do not include limitations on cracking in a mixture. A comparison of Superpave mixes of varying gradation by use of laboratory testing would help in establishing a standard for cracking resistance in asphalt concrete. Although few researchers have done fracture tests on asphalt concrete specimens with a narrow band of air void contents, for example, 7 ± 1% [1-3], it will be interesting to examine the effects of air void content on crack initiation and propagation by examining cracking behavior of specimens prepared at two air voids with large variation (4% vs. 7%).

It is known in the asphalt industry that wet and dry asphalt pavements do not behave identically. There are number of tests to determine the moisture damage behavior of asphalt concrete but there is no test for moisture cracking behavior of asphalt concrete. For example, diametral indirect tension test (AASHTO T-283 [4]) is widely used to conduct a moisture damage assessment on asphalt concrete mixes of various types during Superpave mix design stage. This procedure involves a freeze thaw process analogous to moisture conditions and temperature changes that occur in the field. Both the moisture conditioned and dry cylindrical specimens are loaded in diametral compression and peak loads are compared. It would be interesting to apply this moisture damage process to notched fracture testing samples to examine the effects of moisture damage on crack initiation and propagation. The nature of crack initiation and crack propagation in wet asphalt concrete is not well understood, and a standard method for determining an asphalt concrete design's resiliency to cracking under wet condition has not been established. In deed, the authors have found no studies of fracture in moisture conditioned samples in the literature.

Background

Cracking is a huge issue for asphalt pavements and therefore, it has been studied extensively by many researchers [1, 5-11]. Some researchers have considered asphalt concrete (AC) as a linear elastic material and applied linear elastic fracture mechanics (LEFM) principles [3, 12-15]. Some researchers have idealized the viscoelastic behavior of AC as nonlinear elastic and applied elastic–plastic fracture mechanics (EPFM) concepts to the fracture [16-19]. LEFM and EPFM theory has lead to parameters such as the critical stress intensity factor, K_C, and the fracture energy, J_C, respectively.

[1] Assistant Professor, Department of Civil Engineering, University of New Mexico, Albuquerque, NM 87131, USA.
[2] Graduate Research Associate, Department of Civil Engineering, University of New Mexico, Albuquerque, NM 87131, USA.
[3] Professor, Department of Civil Engineering, University of New Mexico, Albuquerque, NM 87131, USA.
[+] Corresponding Author: E-mail *tarefder@unm.edu*
Note: Submitted August 31, 2008; Revised March 9, 2009; Accepted March 31, 2009.

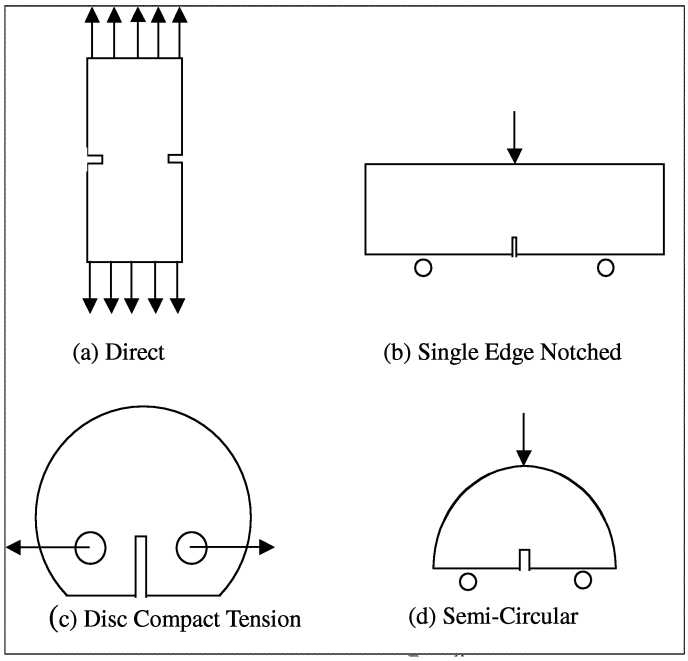

Fig. 1. Common Specimen Geometries for the Study of Fracture in Asphalt Concrete.

For examples, Dongre et al. [20] studied the fracture in asphalt concrete by means of both LEFM and EPFM. These authors concluded that K_C, showed no sensitivity to the mix variables while J_C showed promise as a fracture parameter. Mull et al. [13] used the J-integral concept to evaluate modified asphalt pavement. Quantification of K_C, J_C, or J-integral parameters requires advanced analysis (i.e. finite element analysis) and may not be suitable in a laboratory setting for mix design checking. On the contrary, cracking parameters that are derived directly from load and displacement data may be advantageous. In this paper, opposed to advanced numerical analysis, emphasis is placed on parameters that can be immediately extracted from the load displacement curve such as the ultimate load, crack opening displacement (COD) at ultimate load, cracking potential, fracture load, crack velocity, and slope of the crack propagation curve. The goal is evaluation of crack initiation and propagation using simple, fundamental parameters.

To date, several fracture tests have been developed to study the cracking behavior in HMA under different sample geometries, loading configurations, and material properties [8, 21-25]. In most tests, a notch has been introduced into the sample so that the crack will initiate at the notch. There are four basic sample geometries that were considered for the study of fracture in AC: the direct tension sample, the single-edge notched beam sample, the disc-shaped compact tension sample, and the semi-circular bending specimen [2, 18, 26-30]. These sample geometries are shown in Fig. 1. Fig. 1(a) shows a direct tension (DT) beam shaped specimen that is notched through the width of both lengths of the specimen. Test results from this specimen are highly dependent upon the fabrication and test setup. Even if the notches are cut into the specimen symmetrically, a difference in stress intensity at opposing notch tips can lead to different crack growth rates from each crack. Also, this specimen geometry is dependent upon gluing the ends of the sample to the loading apparatus, which is time consuming and prone to failure. For these reasons, studies applying this specimen geometry are limited in number [1]. Fig. 1(b) shows a single-edge notched beam (SEB) specimen shown in a beam shaped with a rectangular cross section. This specimen is advantageous to use in fracture studies because of its potentially large fracture area. However, obtaining field samples of single-edge notched beam samples is difficult [17, 31]. The disk-shaped compact tension (DCT) specimen is shown in Fig. 1(c). The DCT sample can be prepared by slicing a Superpave gyratory compactor sample or cylindrical core taken from an in-service pavement. The DCT sample can be fabricated from field cores and it allows for a large fracture area. The downside to this sample is the possible deviation of the crack from the line of symmetry due to the incorrect placement of the support holes. Since sample fabrication requires precision, dependency of test results on sample preparation is high [32].

The semi-circular bending (SCB) specimen is shown in Fig. 1(d). The SCB specimen can be fabricated from Superpave gyratory sample or field cores [33]. The specimen is loaded in a three point bending configuration, so the asymmetric loading problem associated with the DT sample is eliminated. This SCB test provides moderate fracture area and a better resolution in the test data [25]. Recently, several researchers suggested the semi-circular bending test set-up using un-notched samples to determine tensile strength of AC in an effort to replace the diametral indirect tension test on cylindrical sample [2, 8, 15, 26]. Krans et al. [34] compared the SCB specimen to other the other possible crack investigation geometries: DCT, center cracked tension sample, and indirect tension sample in three and four point bending. Their study concluded that the SCB specimen is a viable candidate for quality control of mix and pavement design. Hofman et al. [14] conducted static and cyclic experiments on SCB samples. They observed the crack propagation using a video recorder and measured the crack length using a standardized ruler at different times during testing. Their study described the difficulty of measuring the crack length by means of four methods: crack foil, crack opening displacement (COD), mortar displacement, and optical capture by digital camera. The study concluded that measuring crack length for the determination of crack length increase per load cycle was very challenging and not very accurate, although the digital camera method excelled by capturing the bifurcating structure of the cracks. In our study, to eliminate experimenter subjectivity of the video technique, linear variable differential transducers (LVDTs) are used at different locations of an AC sample to determine the crack propagation within the sample.

In this study, semi-circular notched specimens were tested under monotonic loading in strain-controlled mode and crack width is recorded in real time. As a crack propagates in AC, the crack has two measurable quantities that can be observed: the crack width and the crack length. This study captures the crack width in real time at three designated locations away from the notch tip using LVDTs. The crack length is measured using the times history of the LVDT data. A method has been introduced for the first time in this paper to determined crack velocity from the LVDT data. Also, crack path in each specimen is correlated to the aggregate gradation of three Superpave mixes.

Objectives

The goal of this study is to assess the ability of laboratory testing parameters to characterize initiation and propagation of cracks in the semi-circular AC samples. The specific objectives of this study are to:

- Measure crack initiation and propagation in AC samples in real–time using LVDTs.
- Examining the effects of mix type, moisture condition, and void ratio on laboratory crack initiation and propagation parameters such as crack initiation load (P_{int}), ultimate load (P_{ult}), opening displacement at ultimate load (COD_{ult}), the crack velocity (v), and the slope of the crack propagation curve (θ).

Sample Preparation and Testing Procedures

Materials Collection

Three Superpave mixes were collected from a local plant in cooperation with the New Mexico Department of Transportation. Mixes were selected to cover both fine and coarse mixes used in New Mexico. Fig. 2 is an aggregate distribution chart for the three mixes used in this study. Maximum density lines are plotted for both maximum aggregate sizes present. The maximum density lines represent theoretical gradations that will result in maximum density. It is shown in Fig. 2 that mix SP-C has a smaller maximum aggregate size than mixes SP-B and SP-III. Here SP stands for SuperPave or Superior Performing (SP) mixes. Mix gradations that plot above the maximum density line tend to be fine mixes, while gradations below the maximum density line tend to be coarse mixes. The maximum density lines for maximum aggregate sizes of 1.5*cm* (3/4*in*) and 2.54*cm* (1*in*) are plotted in Fig. 2. SP–C has a maximum aggregate size of 1.5*cm* where as mixes SP-B and SP-III both have a maximum aggregate size of 2.54*cm*. Mixes that plot above the maximum density line are generally fine mixes while mixes that plot below the maximum density line are generally coarse mixes. Superpave mixes SP-B and SP-C plot above their respective maximum density lines and mix SP-III plots below its respective density line. Therefore, mix SP-III is a coarse mix and mixes SP-B and SP-C are fine mixes. Of the fine mixes, SP-B is coarser than SP-C.

Binder content, type, and indirect tensile strength values of these mixes are given in Table 1. It can be seen that the moisture conditioned specimens yield lower peak loads than dry samples in indirect tension test (AASHTO T-283 [4]). The polymer modified binders are designated as Superpave performance grade (PG) binders of PG 70-22 and PG 76-28. It can be noted that polymers are mixed with base asphalt binders to create PG binders so that its resistance to flow (viscosity) is less affected by temperature change. The PG 70-22 binder is expected to have small permanent deformation up to 70°C (usually in summer), whereas it is expected to show small low-temperature cracking up to -22°C (usually in winter). The PG 76-28 is good for pavement temperature as high as 76°C and as low as -28°C.

Notched Sample Preparation

Each of the mixes is compacted into 15.25*cm* (6*in*) diameter cylinders by a Superpave gyratory compactor using 600*kPa* (87.02*psi*) vertical pressure (AASHTO T-312 [35]). Sample height

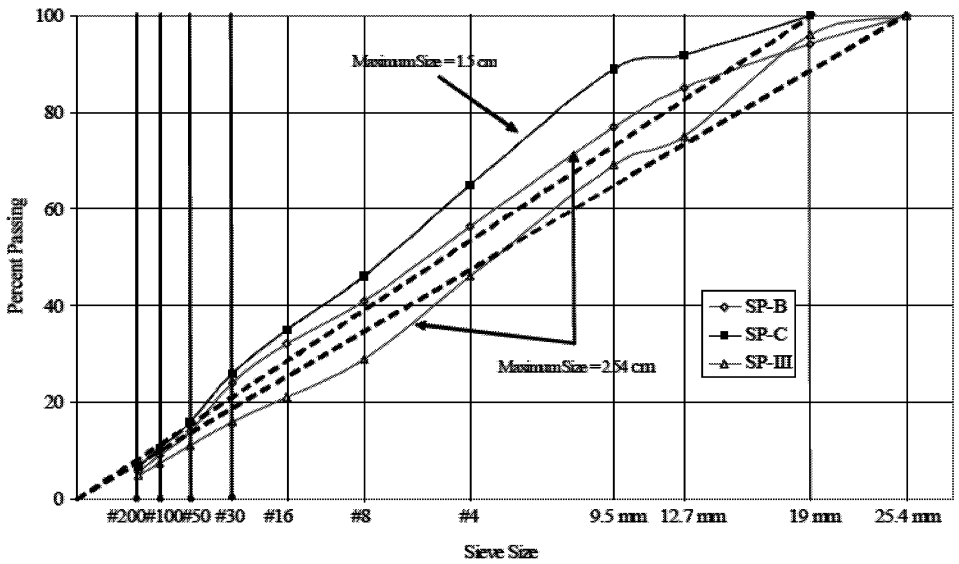

Fig. 2. Aggregate Gradation for Superpave Mixes SP-B, SP-C, and SP-III.

Table 1. Properties of Superpave Mixes.

Superpave Mix Properties	SP-B	SP-C	SP-III
% Optimum Binder	5.6	5.9	5.3
Binders' Performance Grade (PG)	PG 70-22	PG 70-22	PG 76-28
Dry Tensile Strength, *kpa*	951.51	703.29	923.93
Wet Tensile Strength, *kpa*	896.35	655.03	854.98
Tensile Strength Ratio, TSR (AASHTO T-283)	94.2%	93.2%	92.2%

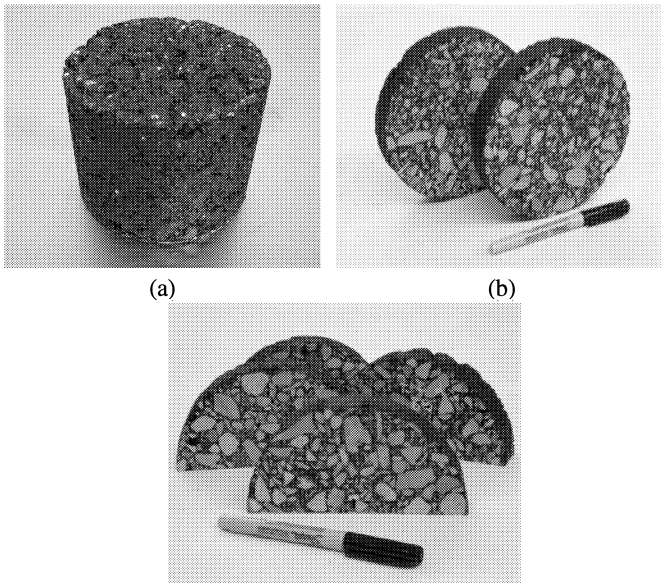

(a) (b)

(c)

Fig. 3. Notched Sample Preparation (a) 6*in* (15.25*cm*) Diameter Sample, (b) Sliced Samples, and (c) Notched Samples.

is kept to 12.7*cm* (5.0*in*). Next, using a water-cooled laboratory saw, two one-inch thick discs are sliced from the center of each cylinder in an attempt to acquire samples with uniform air voids. Finally, the discs are halved and notched in the center of the flat edge with 3/8*in* (9.525*mm*) deep slits using a laboratory saw of 1/8*in* (3.175*mm*) blade thickness. Figs. 3(a), 3(b), and 3(c) show the compacted AC cylinder, sliced discs, and notched samples, respectively.

Test Matrix

Table 2 shows the test matrix and the distribution for the 36 specimens evaluated. Specimen properties highlighted in this analysis include mix type, void ratio, and the moisture condition. It can be seen that the samples are classified into three air void ratios, which are below 4%, above 7%, and in between 4 to 7%. The void ratio of each notched sample is determined using ASTM D-2726 method [36]. It is extremely difficult to prepare samples, which have exact 4% or 7% air voids. Therefore, a number of samples were prepared and notched. Only the ones that satisfied this definition of target air voids were kept. One set of samples was kept dry and the other set was subjected to moisture conditioning. Vacuum saturation and moisture conditioning followed AASHTO T-283 [4] conditioning procedure. Average of the two replicate samples are used in data analysis.

Sample Testing

Table 2. Test Matrix.

Superpave Mix Type	Air Voids	Condition	Sample
SP-B	<4%	Wet	Two
SP-C	4%<e<7%	Dry	Replicates
SP-III	>7%		

Test Matrix =3 Mix × 3 Air Voids × 2 Moisture Conditions × 2 replicates =36 samples

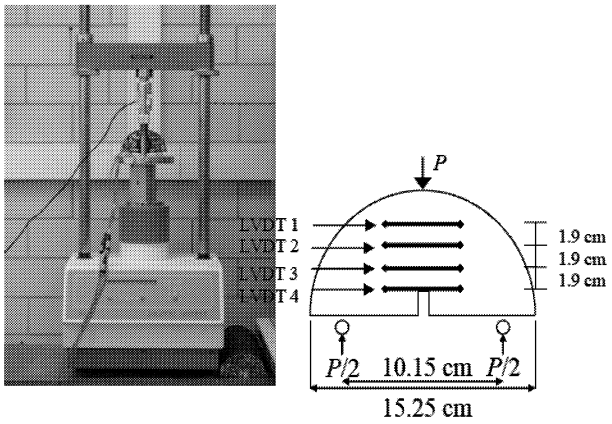

(a) (b)

Fig. 4. Sample Loading Configuration and LVDT Placement (a) Sample Under Load and (b) LVDT Placement.

The loading configuration for the notched sample (SP-B, dry) is shown in Fig. 4. It can be seen that four LVDTs are mounted 0.75*in* (19.05*mm*) above one another beginning at the notch tip in order to measure horizontal displacement at different locations on the sample. Because the horizontal displacement tended to diminish toward the upper portion of the sample the LVDTs are ordered in decreasing range from the bottom edge of the sample to the top loading point. The ranges of the LVDTs are 6.35*mm*, (0.25*in*), 2.54*mm* (0.1*in*), 2.54*mm*, and 0.127*mm* (0.005*in*).

The sample is loaded vertically at a constant strain rate of 0.01*in/min* (0.254*mm/min*). This loading rate was determined based on trials at different rates. It was found that a rate of 0.01*in/min* (0.254*mm/min*) is optimal in inhibiting cracking at the supports while inducing cracking at the notch tip. The LVDTs are mounted using epoxy and connected to the LabVIEW Data Acquisition (DAQ) system. The LVDTs are mounted around a narrow region above the notch point so as to detect only the strain and crack opening displacement directly associated with crack initiation and propagation. The wet samples are allowed to surface dry for approximately five minutes to promote sufficient adhesion to the LVDT mounting blocks. Samples are loaded until the sample develops a visible crack or fracture.

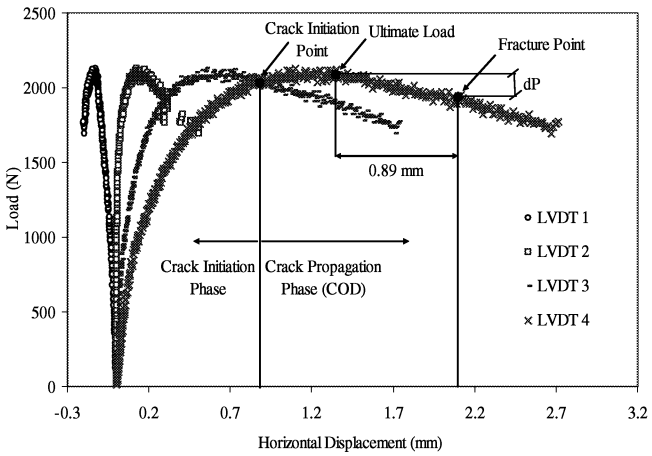

Fig. 5. Load versus Displacement for One Sample of Mix SP-B.

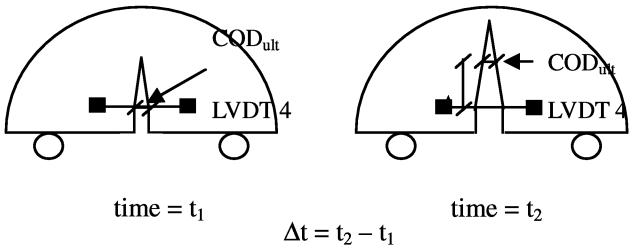

Fig. 6. Schematic of the Locations of Same Amount of COD_{ult} in Δt, the Time Difference.

Analysis of Test Results

Fig. 5 is the load versus horizontal displacement data for four LVDTs for a sample of mix SP–B. The load versus horizontal displacement curve in Fig. 5 is divided into two portions: the crack initiation phase and the crack propagation phase. The portion of the loading curve beginning at the onset of loading up to the crack initiation load is the crack initiation phase of the cracking process. In this phase micro cracks and micro voids are formed without reduction in loading. The crack becomes visible at the crack initiation load (P_{int}), which is defined as the crack initiation point. This value is determined by laboratory observation. Any increase in the horizontal displacement after crack initiation is considered actual crack width, or crack opening displacement. The sample continues to sustain increasing load as the crack propagates through the sample. The sample attains ultimate load (P_{ult}) at maximum point of the load versus displacement curve. The corresponding COD is defined as COD_{ult}. After which, the load starts to decrease as the COD increases. A finite crack is visible in all samples when LVDT 4 measures a COD value of 0.035*in* (0.9*mm*) after the COD value at ultimate load. In this study fracture is defined when COD_{ult} + 0.035*in* (0.9*mm*) is reached at LVDT 4. From laboratory observation, the authors discovered that in some of the samples, if testing continued 0.035*in* (0.9*mm*) beyond COD_{ult} several cracks occur in the sample.

While P_{int} can be used as a measure of crack initiation and P_{ult} indicates the overall strength of the sample, the difference between the ultimate load and the crack initiation load (P_{ult} - P_{int}) is used to characterize a sample's resistance to failure due to cracking. For example, a sample that can withstand 222*N* (50*lbs*) additional load after crack initiation as opposed to 20*lbs* (89*N*) additional load has a higher strength in the presence of cracking.

Two parameters are used to characterize propagation: the crack velocity (v) and the slope of the crack propagation curve (θ). The slope of the crack propagation curve (θ), is the change in load (dP) for a COD value of 0.035*in* (0.9*mm*) past the COD at ultimate load as shown in Fig. 5.

Crack Velocity

Crack velocity is calculated from the COD and time. In this paragraph, the method of determining crack velocity is described. Crack velocity is defined as the distance traveled by the crack (Δl) divided by the time elapsed. That is:

$$v = \frac{\Delta l}{\Delta t} \quad (1)$$

where v = velocity, Δl = crack length, and Δt = time elapsed. Fig. 6 shows a schematic of a crack (same width) appearance at two difference locations. At time, t = t_1 the crack initiates (COD = COD_{ult}) at the crack tip or LVDT 4. From the data acquired, the time (t = t_2) can be recorded when the same width (COD_{ult}) appears at the LVDT 3 location. As a result, $\Delta t = t_2 - t_1$ and distance traveled by the crack, Δl = 0.75 (distance between the LVDT 4 and 3). Velocity can be calculated by using these values in Eq. (1), however, this is an average velocity in the region between LVDT 4 and 3. For a continuous velocity profile, time series of data collected by LVDTs is used to find the distance traveled by the crack of same width (i.e. COD_{ult}). The following paragraph explains how the time series of LVDT data is used to determine the distance traveled by the crack.

The four LVDTs implemented in this study detect the presence of the crack by reading out a value for horizontal displacement equal to COD_{ult}, which is the crack initiation width for a given sample. When this value is detected in subsequent LVDTs as the crack propagates, the distance traveled by the crack can be determined with reference to time or load. For example, when COD_{ult} LVDT 3 measures, the crack is considered to have traveled 1.91*cm* (0.75*in*) from LVDT 4 to LVDT 3. Based on this principle, it is possible to interpolate the location of the crack initiation point, or the length of the crack, at any given time. This is accomplished by use of a chart shown in Fig. 7.

In Fig. 7, half of the horizontal displacement is plotted as a function of distance from the notch tip in a sample of mix SP-B. Each line is plotted using four data points, one from each LVDT at a given time. In order to interpolate the crack length a horizontal line is drawn through the COD value (0.015*in* (0.4*mm*)) at LVDT 4 corresponding to crack initiation, COD_{ult}. The intersection of this horizontal line with any one of the other lines is considered as the location of the crack tip at that time interval. The distance of such intersection points from the origin are noted as the distance from the notch tip to the crack tip, or the distance traveled by the crack. The vertical dotted lines are plotted in Fig. 7 show the increasing distance traveled by the crack tip at equal time intervals. Crack velocity is calculated using this distance at different time intervals. It is clear as the crack travels from the notch tip to the top of the sample that the velocity of the crack decreases.

Fig. 7 can be exploited in order to understand three different regions along the crack propagation path: the compression region, the tensile deformation region, and the crack-widening region. The compression region in the sample denotes locations where the LVDT has recorded negative COD values. The tensile deformation region in the sample is located where no crack is present (below the horizontal line where COD = 0.015*in*(0.4*mm*) = COD_{ult}), but positive values are recorded by the LVDTs. The crack widening region is above the horizontal line passing through the COD at the crack initiation point. From Fig. 7, it is evident that there is no linear relationship between crack widening and crack growth.

Repeatability Study

Repeatability of sample preparation and testing procedure was evaluated by preparing six specimens of similar mix type (SP-B), and air void content (4±1%). Three of the samples were soaked in water for 24*hrs* prior to testing and three were kept dry. Table 3 presents

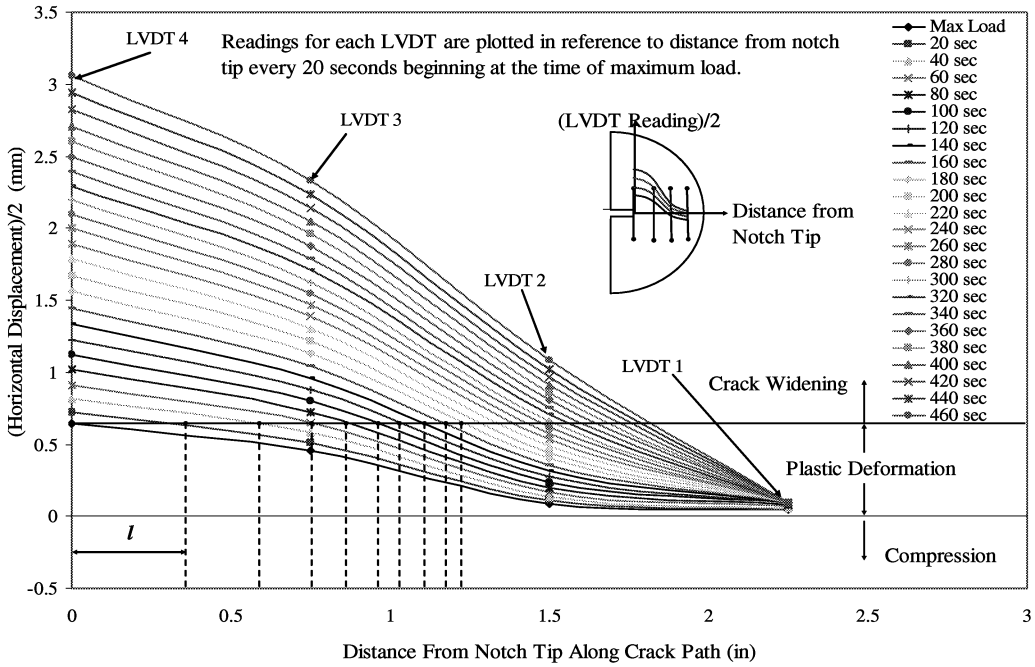

Fig. 7. LVDT Reading vs. Distance from Notch Tip at 20*sec* Intervals.

Table 3. Repeatability Analysis.

Sample ID	Ultimate Load (P_{ult}, *N*)	COD at Ultimate Load (COD_{ult}, *mm*)	Crack Initiation Potential (*U*, *N*×*mm*)	Fracture Load (P_f, *N*)	Slope of Crack Propagation Curve (*q*, *N*/0.89 *mm*)	Initial Crack Velocity (*v*, *mm/min*)
Wet 1	2095	0.44	1039	1744	507	8.4
Wet 2	1766	0.43	667	1423	494	8.1
Wet 3	2064	0.49	847	1806	454	6.6
Average	1975	0.45	851	1658	485	7.7
Standard Deviation	182	0.03	186	205	28	1.0
Coef. of Variance (%)	11	7	22	12	6	13
Dry 1	2206	0.58	1220	2144	280	10.9
Dry 2	2095	0.50	825	2015	258	12.2
Dry 3	2326	0.52	1299	2242	223	13.0
Average	2209	0.53	1115	2134	254	12.0
Standard Deviation	116	0.04	254	114	29	1.0
Coef. of Variance (%)	5	8	23	5	11	9

data from the testing of these specimens. The table includes: ultimate load, COD at ultimate load, crack initiation potential, fracture load, slope of the crack propagation curve, and initial crack velocity. For each parameter the standard deviation and coefficient of variation is calculated. It can be seen in the table that the coefficient of variation (COV) is less that 15% for all parameters other than the crack initiation potential. Fifteen percent is similar to COVs calculated for tests on SC(B) samples by Tolman and Herder [33] and Li and Marasteanu [15].

Crack Path Study

Crack path was observed in each of the samples tested in order to determine the preferred path of crack propagation. Fig. 8 shows three frames from a video taken during the test of a sample of mix SP-B. Fig. 8(a) shows initiation of the crack at the notch tip, the white coloring is a chalk mark that aided in the visibility of the crack initiation. Fig. 8(b) shows the crack as it has propagated away from the notch tip.

Fig. 8 shows crack propagation paths captured during the specimen testing. It can be seen that the crack tends to travel along the interface between the mastic and aggregate material.As an interface becomes less preferential, the crack is shown to transfer directly to another interface. Fig. 8(c) shows the wandering of a crack in the instance where there is no interface in the vicinity of crack propagation. The crack appears to have a less defined pathway in the absence of an interface.

Results and Discussion

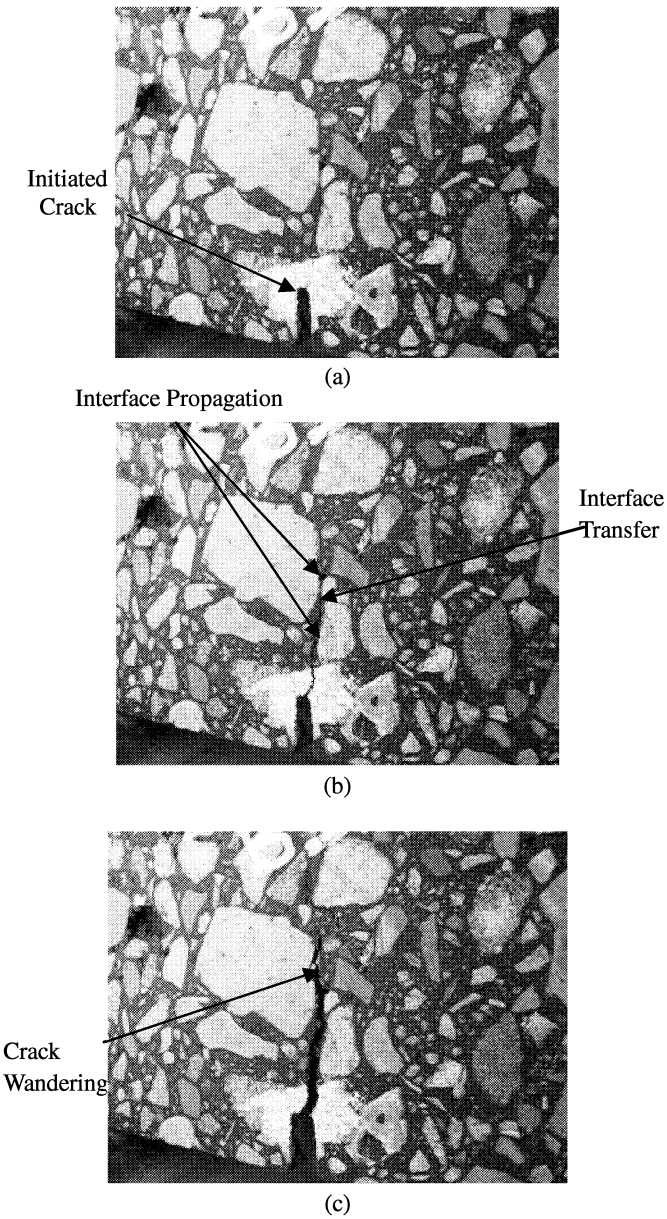

Fig. 8. Crack Propagation Path from Sample Testing (a) Hairline Crack Initiation (b) Crack Propagation along Interfaces, and (c) Crack Wandering through the Mastic.

Table 4. Regression Equations and R-Squared Values for Parameters P_{ult} and P_{int}.

	Ultimate Load, P_{ult}	Crack Initiation Load, P_{int}
Wet and Dry	$y = 0.4437x^2 - 12.663x + 348.21$ $R^2 = 0.1674$	$y = 1.6727x^2 - 27.707x + 335.64$ $R^2 = 0.2498$
Dry	$y = 0.2967x^2 - 6.7651x + 306.62$ $R^2 = 0.1146$	$y = 0.0679x^2 - 5.2799x + 271.71$ $R^2 = 0.1516$
Wet	$y = 3.8656x^2 - 55.134x + 453.41$ $R^2 = 0.4717$	$y = 1.264x^2 - 30.332x + 354.54$ $R^2 = 0.4823$

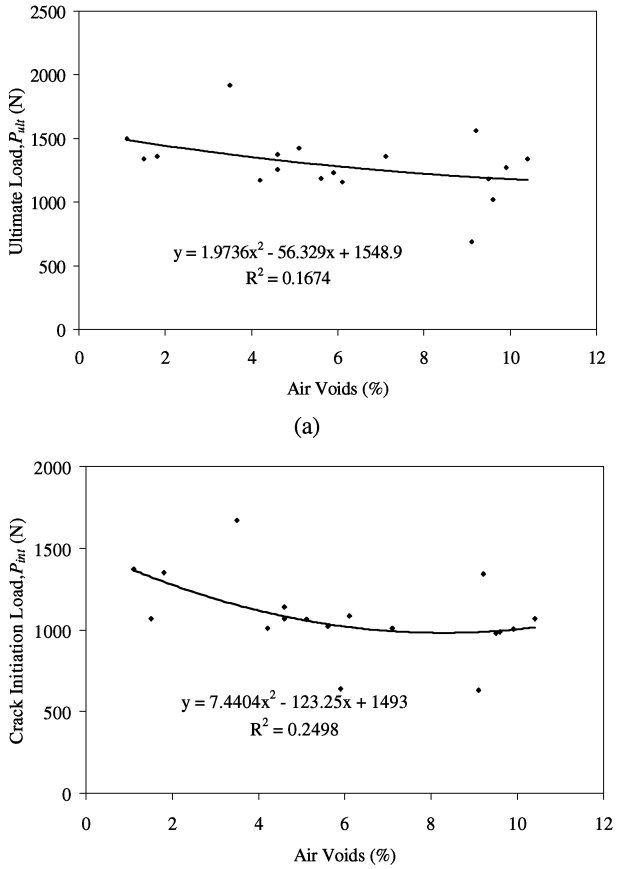

Fig. 9. (a) Ultimate Load versus Air Void Percentage and (b) Crack Initiation Load versus Air Void Percentage.

Effect of Air Voids on P_{ult}, P_{int}, and v

Fig. 9 shows scatter plots of the ultimate load (P_{ult}) and the crack initiation load (P_{int}) versus air voids for each sample tested in this study. A second order trend line is fit to the data in each plot. The equation for the trend line and the coefficient of variation is displayed on each plot. Similar plots can be made for the only wet and dry samples respectively for the ultimate load and the crack initiation load. The equations for the trend lines and the R^2 values for these plots are listed in Table 4. The coefficient of variation (R^2), is significantly less than unity for each plot, although the R^2 for the wet samples only is near 0.5 for both P_{int} *and* P_{ult}..

Fig. 10(a) shows the crack velocity versus the crack length in mix SP-B for three dry samples of varying void ratio and three wet samples of varying void ratio. It can be seen from the plot that the samples of low and medium air void ratios show similar trends in crack velocity. The velocity starts highest at an initial value of about10*mm/min* for the wet samples and about 15*mm/min* for the dry samples, and then decreases at similar slope until the end of the test. The samples with the highest void ratio exhibit higher initial crack velocity. The crack velocity in the high air voids samples appears to be most variable. It is possible that the increased amount of air voids in a sample leads to an increase in crack velocity by providing a crack pathway that requires less actual fracture of material. From Fig. 10(b) it can be seen that wet samples generally

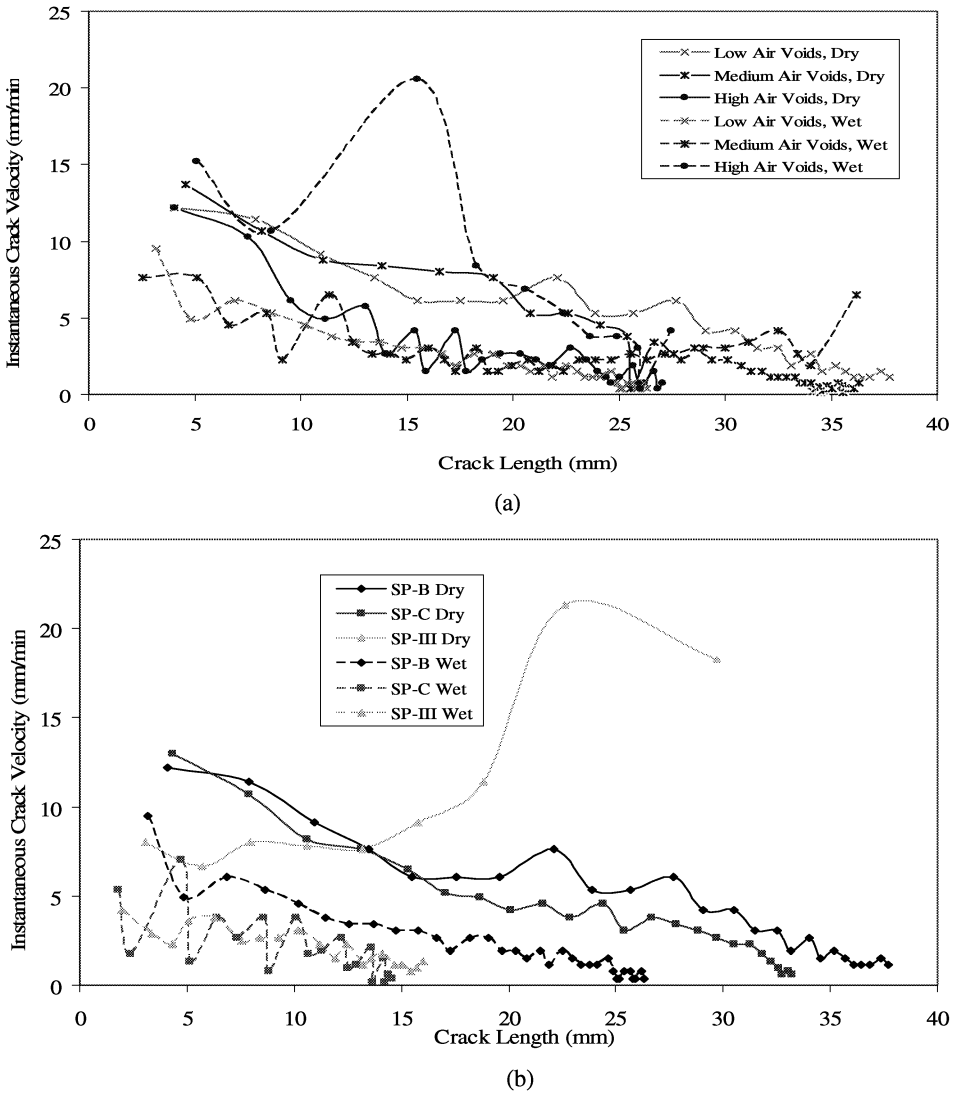

Fig. 10. (a) Effect of Air Voids on Crack Velocity (SP-B) and (b) Effect of Moisture and Mix Type on Crack Velocity.

Table 5. Cracking and Loading Parameters for Each Sample.

	Air Voids	Moisture	COD_{ult}	P_{ult} (N)	P_{int} (N)	P_{ult}-P_{int}
SP-B	e<4	DRY	2.13	1259	1068	191
	4.6	WET	1.35	1375	1139	236
	4<e<7	DRY	0.30	1161	1085	76
	5.6	WET	1.65	1188	1023	165
	e>7	DRY	0.41	1272	1005	267
	9.1	WET	1.02	694	632	62
SP-C	e<4	DRY	0.43	1499	1370	129
	1.5	WET	0.71	1343	1068	271
	4<e<7	DRY	0.71	1170	1010	160
	5.9	WET	1.75	1232	641	592
	e>7	DRY	0.36	1183	983	200
	10.4	WET	0.71	1339	1068	271
SP-III	e<4	DRY	0.05	1361	1352	9
	3.5	WET	0.23	1922	1668	249
	4<e<7	DRY	0.33	1361	1010	351
	5.1	WET	0.23	1428	1063	365
	e>7	DRY	0.18	1019	988	31
	9.2	WET	0.28	1561	1343	218

exhibit slower cracks. The moisture damage process softens a sample, creating more ductility that allows for greater amounts of bending before fracture.

Effect of Moisture on COD_{ult}, P_{ult}, P_{int}, and v

Table 5 has a list of values for the difference between the ultimate load and the crack initiation load (P_{ult} - P_{int}). It can be seen from these load difference values that the values for wet samples are consistently higher than those for the dry samples. This trend indicates that after cracks have initiated in AC, wet samples will withstand failure better than dry samples. This is a cohesive type failure where sample wetting after certain extent increases the bond strength, thereby wet samples are more ductile than dry samples.

Fig. 11 is a bar chart that shows the average crack openingdisplacement at ultimate load for all dry and wet samples of each mix type evaluated in this study. Each bar is the average COD_{ult} for samples of all void ratios. The averaged range of the samples is shown with the error bars. The COD at ultimate load (COD_{ult}) is an indication of the amount of cracking necessary to

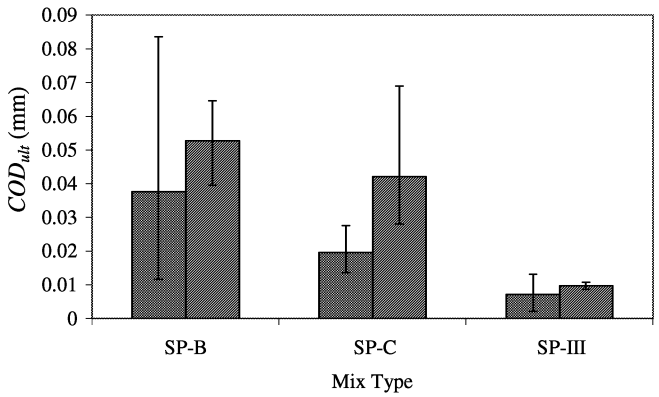

Fig. 11. Crack Opening Displacement at Ultimate Load for Dry and Wet Samples.

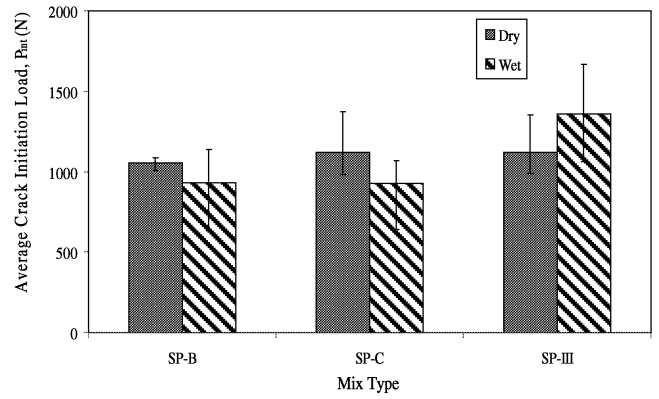

(a)

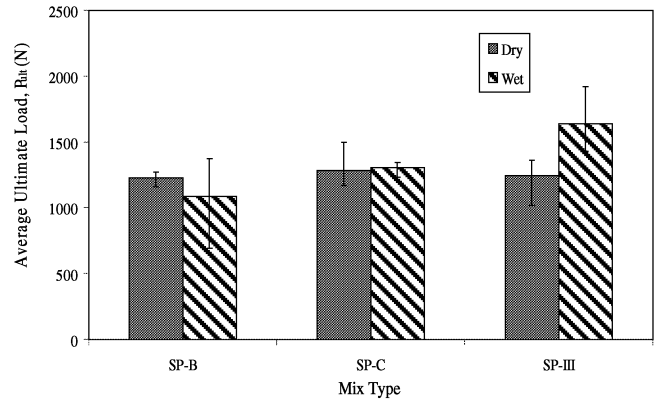

(b)

Fig. 12. (a) Average Crack Initiation Load and (b) Average Crack Initiation and Ultimate Loads for Dry and Wet Sample.

induce failure in a sample. Fig. 11 indicates that, in general, wet samples experience higher COD at ultimate load than dry samples. Based on the average of the result, the average COD for the dry samples of all mix types is 0.021*in* (0.5*mm*) and the average COD for the wet samples of all mix types is 0.89*mm*. So, the moisture damage process facilitates the widening of cracks up to the point of ultimate load. More consistent results are found for the coarse mix, mix SP-III.

Fig. 11 also shows that the highest values for COD_{ult} occur in mix SP-B while the lowest values occur for mix SP-III. Mix SP-B is a

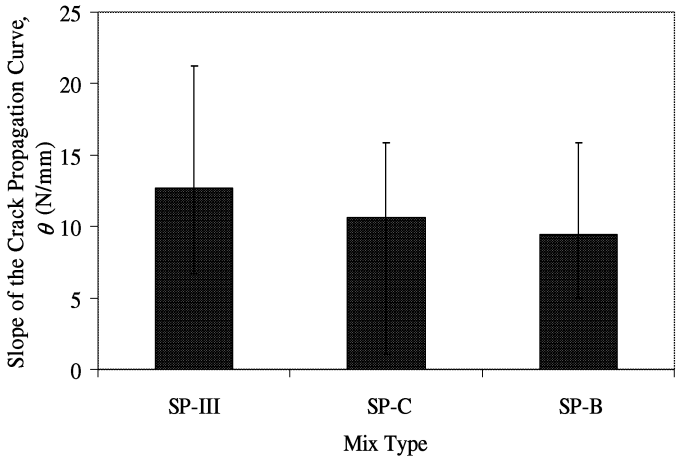

Fig. 13. Average Slope of the Crack Propagation Curve for Each Superpave Mix Type.

fine mix with a softer binder than the coarse mix SP-III. A softer binder results in greater ductility, so greater amounts of displacement should be expected in mix SP-B than mix SP-III. Mix SP-B contains a larger percentage of coarse aggregate than mix SP- C. The interface existing between coarse aggregate and mastic material is susceptible to damage and could allow for increased COD when compared to a sample with less coarse aggregate.

Fig. 12(a) and 12(b) show the average crack initiation load and average ultimate load for wet and dry samples of each mix type. Each bar is the average P_{int} for samples of all void ratios. The error bars show the range of the samples averaged. Fig. 12(a) shows that the crack initiation load for dry samples in mixes SP–B and SP-C was higher, while the crack initiation load in mix SP–III is higher for wet samples. This trend indicates that dry samples will take more loads before crack initiation. This is expected since moisture is known to damage asphalt concrete. From Fig. 12(b), the ultimate load for the wet samples is higher than or comparable to the ultimate load for dry samples. The average of the ultimate load for the wet samples is 1,345*N* (302*lbs*), while the ultimate load for the dry samples is 1,254*N* (282*lbs*). The moisture damage in asphalt concrete results in increased ductility. The ductility in the sample allows for higher levels of strain. When the sample is strained the sample hardens as the air voids close.

Effect of Gradation on P_{int}, P_{ult}, v, and θ

Figs. 12(a) and (b) show the average P_{int} and P_{ult} for wet and dry samples of each mix type with the range of samples tested denoted by error bars. For the average crack initiation load, it can be seen in Fig. 12(a) that mix SP-III generally has the highest average crack initiation load. Distinct differences between mix SP-III from mixes SP-B and SP-C are the stiffer binder contained in mix SP-III and the high percentage of coarse aggregate. Either of these two mix characteristics could be contributing to the observed trend.

Consider the average ultimate load for each mix type shown in Fig. 12(b). There is a general trend of increasing ultimate load and crack initiation load with SP-B being the lowest in load, and SP–III being the highest. This is explainable because mix SP-III is a coarse mix that is expected to withstand larger loads. Of the two finer

mixes, SP-B and SP-C, SP-B contains a higher percentage of coarse aggregate and therefore more interfaces along which a crack can continuously propagate.

In Fig. 10(a), the crack velocity reveals no clear trend between aggregate gradation and cracking. Although one might expect that crack velocity could be highest in coarser samples due to interface cracking.

Fig. 13 shows the average slope of the crack propagation curve for each mix type. The values shown are averages of all samples of each mix type. Mix SP-III has the greatest slope and mix SP-B has the smallest slope. The slope of the crack propagation curve (θ) is a measure of a sample's resilience to cracking damage as the crack width increases. In that respect, the coarse mix has the least resistance to cracking damage. Preferred cracking along aggregate-mastic interfaces may indicate that the bond along the interface is weaker than that inside the mastic or aggregate. The large load decrease observed in mix SP-III can then be explained by realizing that mix SP-III is a coarse mix with large continuous interfaces along which cracks can propagate. These quasi-continuous crack path-ways facilitate extensive crack propagation and therefore high structural damage that leads to a decrease in load carrying capacity.

One might suspect that if coarse aggregate present in a mix leads to a large load decrease then mix SP-B should exhibit a larger load decrease than mix SP-C. The average value of load decrease for mix SP-C is somewhat misleading because one value is extremely high, while the remaining values are generally less than 90*N* (20*lb*). If the outlying value for SP-C is overlooked, the average load decrease decreases to 152*N* (34*lb*).

Conclusion

- Air voids had very little to no effect on the crack initiation load or the ultimate load. Specimens with greater air voids showed higher velocity than specimens with lesser air voids.
- Wet samples sustained fewer loads before crack initiation than dry samples. Wet samples sustained higher ultimate loads than dry samples. Also, wet samples showed slower cracks than dry samples, suggesting that wet pavements will have a longer service life.
- The coarse mix in this study failed at higher loads than the fine mixes. Mixes with more coarse aggregate allow for continuous crack propagation along aggregate-mastic interfaces, leading to steeper unloading curves after the ultimate load. All three mixes showed similar crack velocities.
- The interface pathway is preferential for crack initiation and propagation.

Acknowledgements

This project is funded by the National Science Foundation (NSF). NSF grant number: 0644047 and Program: Infrastructure Materials & Structural Mechanics. Thanks to Mr. Robert Meyers and Mr. Parveez Anwar of NMDOT for their advice during the project. The authors appreciate the assistance provided by Mr. John Galvin of the Lafarge North America Quality Assurance Laboratory in obtaining the material needed for this study.

References

1. Jacobs, M.M.J., Hopman, P.C., and Molenaar, A.A.A., (1996). Application of Fracture Mechanics Principles to Analyze Cracking in Asphalt Concrete, *Asphalt Paving Technology*, Vol. 65, pp. 1-39.
2. Van de Ven, M., de Fortier Smit, A., and Krans, R., (1997). Possibilities of a Semi-Circular Bending Test, *Proceedings of the Eighth International Conference of Asphalt Pavements*, Vol. 2, pp. 939-950, Seattle, WA, USA.
3. Zhang, Z., Roque, R., and Birgisson, B., (2001). Evaluation of Laboratory Measured Crack Growth Rate for Asphalt Mixtures, *Transportation Research Record*, No. 1767, pp. 67-75.
4. AASHTO, (2000). Resistance of Compacted Bituminous Mixture to Moisture Induced Damage for Superpave, *AASHTO T-283*, American Association of State Highway and Transportation Officials (AASHTO), Washington DC, USA.
5. Abdulshafi, A.A, and Majidzadeh, K., (1985). J-Integral and Cyclic Plasticity Approach to Fatigue and Fracture of Asphalt Mixes, *Transportation Research Record*, No. 1034, pp. 112-123.
6. Mobasher, B., Mamlouk, M.S., and Lin, H., (1997). Evaluation of Crack Propagation Properties of Asphalt Mixtures, *Journal of Transportation Engineering*, 123(5), pp. 405-413.
7. Roque, R., Birgisson, B, Sangpetgnam, B., and Zhang, Z., (2002). Hot Mix Asphalt Fracture Mechanics: A Fundamental Crack Growth Law for Asphalt Mixtures, *Journal of the Association of Asphalt Paving Technologists*, Vol. 71, pp. 816-827.
8. Molenaar, A., Scarpas, A., Liu, X, and Erkens, G, (2002). Semi Circular Test; Simple but Useful, *Journal of the Association of Asphalt Paving Technologists*, 71, pp. 794-815.
9. Walubita, L.F., Martin, E.A., Cleveland, G.S., and Lytton, R.L., (2006). Computation of Pseudo Strain Energy and Paris Law Fracture Coefficients from Surface Energy and Uniaxial Strain-Controlled Tension Test, *International J. of Pavement Eng.*, 7(3), pp. 167-178.
10. Kim, Y., Lee, H.J., Little, D.N., and Kim, Y.R., (2006). A Simple and Reliable Testing Method to Evaluate Fatigue Fracture and Damage Performance of Asphalt Mixtures, *Journal of Association of Asphalt Paving Technologists*, Vol. 75, pp. 755-787.
11. Li, X, Marasteanu, M., and Turos, M., (2007). Study of Low Temperature Cracking in Asphalt Mixtures Using Mechanical Testing and Acoustic Emission Methods, *Journal of the Association of Asphalt Paving Technologists*, Vol. 76, pp. 427-453.
12. Majidzadeh, K., (1976). Application of Fracture Mechanics for Improved Design of Bituminous Concrete, *Report, FHWA-rd-76-91*, Vol. 1-2, Federal Highway Administration, USA.
13. Mull, M.A., Stuart, K., and Yehia, A., (2002). Fracture Resistance Characterization of Chemically Modified Crumb Rubber Asphalt Pavement, *Journal of Materials Science*, 37(24), pp. 557-566.
14. Hofman, R., Oosterbaan, B., Erkens, S.M.J.G, and van der

Kooij, J., (2003). Semi-Circular Bending Test to Assess the Resistance Against Crack Growth, *Proceedings of the 6th R1LEM Symposium on Performance Testing and Evaluation of Bituminous Materials*, pp. 257-263, Zurich, Switzerland.

15. Li, X. and Marasteanu, M., (2004). Evaluation of Low Temperature Fracture Resistance of Asphalt Mixture Using the Semi-Circular Bend Test, *Journal of the Association of Asphalt Paving Technologists*, Vol. 73, pp. 401-426.
16. Anderson, T.L., (2005). *Fracture Mechanics, Fundamentals and Applications*, Taylor and Francis Boca, Raton, FL, USA.
17. Aglan, H., Othman, A., and Figueroa, L., (1994). Processing Conditions-Fracture Toughness Relationships of Asphalt Concrete Mixtures, *Journal of Materials Science*, 29(18), pp. 4786-4792.
18. Wu, Z., Mohammod, L.N., Wang, L.B., and Mull, M.A., (2005). Fracture Resistance Characterization of Superpave Mixtures Using the Semi-Circular Bending Test, *Journal of ASTM International*, 2(3), pp 1-15.
19. Rice, J.R., (1968). A Path Independent Integral and the Approximate Analysis of Strain Concentration by Notches and Cracks, *Journal of Applied Mechanics*, Vol. 35, pp. 379-386.
20. Dongre, R., Sharma, M.G., and Anderson, D.A., (1989). Development of Fracture Criterion for Asphalt Mixes at Low Temperatures, *Transportation Research Record*, No. 1228, pp. 94-105.
21. Roque, R., Zhang, Z., and Sankar, B., (1999). Determination of Crack Growth Rate Parameters of Asphalt Mixtures Using the Superpave IDT, *Journal of the Association of Asphalt Paving Technologists*, Vol. 68, pp. 404-433.
22. Li, Y. and Metcalf, J.B., (2002). Crack Initiation Model from Asphalt Slab Tests, *Journal of Materials in Civil Engineering*, 14(4), pp. 303-310.
23. Birgisson, B., Roque, R., and Page, G., (2003). Evaluation of Water Damage Using Hot Mix Asphalt Fracture Mechanics, *Journal of the Association of Asphalt Paving Technologists*, Vol. 73, pp. 424-462.
24. Birgisson, B., Roque, R., and Page, G., (2004). The Use of a Performance-Based Fracture Criterion for the Evaluation of Moisture Susceptibility in Hot Mix Asphalt, *Transportation Research Record*. No. 3431, pp. 55-61.
25. Huang, B., Shu, X., and Zuo, G., (2005). Laboratory Evaluation of Semi-Circular Bending Tensile Strength Test for HMA Mixtures, *84th Annual Meeting of the Transportation Research Board*, Washington, DC, USA, No. 05-0130, CD-ROM.
26. Van de Ven, M., de Fortier Smit, A., and Krans, R., (1997). Possibilities of a Semi-Circular Bending Test, *Proceedings of the Eight International Conference of Asphalt Pavements*, Vol. 2, pp. 939-950, Seattle, WA, USA.
27. Chong, K. P. and Kuruppu, M.D., (1984). New Specimen for Fracture Toughness Determination for Rock and Other Materials, *International Journal of Fracture*, Vol. 26, pp. 59-62.
28. Lim, I.L., Johnston, I.W., and Choi, S.K., (1993). Stress Intensity Factors for Semi-Circular Specimens under Three-Point Bending, *Engineering Fracture Mechanics*, 44(3), pp. 363-382.
29. Schapery, R.A., (1984). Correspondence Principles and a Generalized J-Integral for Large Deformation and Fracture Analysis of Viscoelastic Media, *International Journal of Fracture*, 25(3), pp. 195-223.
30. Schapery, R.A., (1989). On the Mechanics of Crack Closing And Bonding in Linear Viscoelastic Media, *International Journal of Fracture*, 39(1-3), pp. 163-189.
31. Wagoner, M.P., Buttlar, W.G., and Paulino, G.H., (2005). Development of a Single-Edge Notched Beam Test for Asphalt Concrete Mixtures, *Journal of Testing and Evaluation*, 33(6), pp 452-459.
32. Wagoner, M.P., Buttlar, W.G., and Paulino, G.H., (2005). Disc-Shaped Compact Tension Test for Asphalt Concrete Fracture, *Experimental Mechanics*, 45(3), pp. 270-277.
33. Tolman, F. and den Herder, A.J., (1999). The Value of the SCB Test for Fracture, *Materials for Buildings and Structures*, Ch. 21, pp. 149-153, edited by Wittmann, F.H., published by Deutsche Gesellschaft für Materialkunde, Wiley-VCH.
34. Krans, R., Tolman, F., and Van de Ven, M.F.C., (1996). Semi-Circular Bending Test: A Practical Crack Growth Test Using Asphalt Concrete Cores, *Proceedings of the 3rd International RILEM Conference on Reflective Cracking in Pavements-Design and Performance of Overlay Systems*, Vol. 1, part 2, pp. 123-133, Maastricht, The Netherlands.
35. AASHTO, (2000). Standard Procedure for Preparing and Determining the Density of Hot Mix Asphalt (HMA) Specimens by Means of the SHRP Gyratory Compactor, *AASHTO T-312*, American Association of State Highway and Transportation Officials (AASHTO), Washington DC, USA.
36. ASTM, (1996). Standard Test Method for Bulk Specific Gravity and Density of Non–Absorptive Compacted Bituminous Mixtures, *Annual Book of ASTM Standards, ASTM D-2726*, Vol. 04.03, Philadelphia, PA, USA.